Applied Catalysis B: Environmental 241 (2019) 338–350

Contents lists available at ScienceDirect

Applied Catalysis B: Environmental

journal homepage: www.elsevier.com/locate/apcatb

Volatilisation and subsequent deposition of platinum oxides from diesel oxidation catalysts

Kirsten Leistner[a], Carolina Gonzalez Braga[a], Ashok Kumar[b], Krishna Kamasamudram[b], Louise Olsson[a,*]

[a] Competence Centre for Catalysis, Chemical Engineering, Chalmers University of Technology, SE-412 96 Gothenburg, Sweden
[b] Cummins Inc., 1900 McKinley Ave, MC 50183, Columbus, IN 47201, USA

ARTICLE INFO

Keywords:
Platinum poisoning
Noble metal volatilization
Palladium
Diesel oxidation catalyst

ABSTRACT

In this study, we have reproduced a DOC-upstream-of-SCR configuration in the laboratory, with washcoated model Pt/Al_2O_3, $Pd\text{-}Pt/Al_2O_3$ and Pd/Al_2O_3 catalysts, as well as a commercial DOC, upstream of an alumina-washcoated core. We studied vapour-phase noble metal poisoning of the alumina core, as noble metal from the model DOC catalysts deposited on the downstream alumina core. The mobile species were predominantly volatile platinum oxides, whereas Pd volatilised in such small traces that it was close or below detection limit by Inductively Coupled Plasma – Sector Field Mass Spectrometry (ICP-SFMS), even when the model DOC had only Pd as active species. Even after volatilisation at temperatures as low as 550 °C, the deposited trace amounts of noble metal were highly active for ammonia oxidation. The deposited platinum appears to be finely dispersed, but when subjected to reaction conditions, it likely undergoes sintering, causing a further increase of the ammonia oxidation ability, which will affect the extent of poisoning in a real exhaust aftertreament system. We investigated the dependence of volatilization on temperature, and, as predicted, found it to be exponential. Exposure to increasing temperatures causes different degrees of sintering of the noble metal particles and we found qualitative evidence that sintering decreases the amount of volatilisation. Adding a small amount of Pd (Pd:Pt = 0.5:1) to the catalyst had no effect on volatilisation. However, larger Pd concentrations (Pd:Pt = 1:1 or 2:1) decrease volatilisation. The results for the model DOCs were confirmed by volatilisation from a commercial DOC, where in fact the capturing core exhibited even higher ammonia oxidation ability compared to those downstream of the model DOCs, after evaporation at 700 °C.

1. Introduction

It has been known for a long time that volatilising platinum group metals (PGMs) from exhaust catalysts can end up downstream of the catalyst, which can cause environmental concerns [1–5]. In 2005, Rauch et al. estimated global catalyst emission of 0.8–6.0 metric tons of Pt/year, assuming that 500 million vehicles are equipped with catalysts with an average yearly mileage of 15,000 km/vehicle and an average emission rate of 0.1–0.8 μg/km [6]. While a large proportion of this is likely due to mechanical attrition losses, rather than volatilisation, the number illustrates the magnitude of the issue. Hence there is clearly a need for improved understanding of the rate of noble metals emitted from automotive exhaust catalysts [6].

More recently, it has been shown that volatilisation from diesel oxidation catalysts (DOCs) also negatively affects selective catalytic reduction (SCR) catalysts, which are typically positioned downstream of the DOC in the exhaust aftertreatment system [7–9]. This noble metal poisoning consists of very small amounts of noble metal deposition on the downstream SCR component [8,9]. Although the amounts are very small, they can severely affect the efficiency of the SCR catalyst, because the noble metal poisoning proceeds through competitive ammonia oxidation, thus not leaving enough ammonia for the SCR reaction to continue, which in turn causes an increase in urea consumption to compensate [7–11]. In addition to the resulting poor NO_x conversion, it causes increased N_2O formation [8,10].

Most of what is known about noble metal volatilisation comes from very different applications, such as Pt-Rh gauzes for the oxidation of ammonia into nitric acid, Pt wires and Pt discs, chemical and physical vapour deposition processes [12–19]. The experimental conditions between these areas of application can differ substantially, hence the measured rate of loss of noble metal can differ by several orders of magnitude [13]. Studying noble metal volatilisation in exhaust

* Corresponding author.
E-mail address: louise.olsson@chalmers.se (L. Olsson).

https://doi.org/10.1016/j.apcatb.2018.09.022
Received 3 June 2018; Received in revised form 29 August 2018; Accepted 8 September 2018
Available online 08 September 2018
0926-3373/

Notations

DOC	Diesel oxidation catalyst
DRIFTS	Diffuse reflectance infrared Fourier-Transform spectroscopy
EDX	Energy dispersive X-ray spectroscopy
ICP-MS	Inductively coupled plasma mass spectrometry
ICP-SFMS	Inductively coupled plasma sector field mass spectrometry
SCR	Selective catalytic reduction
STEM	Scanning transmission electron microscopy
XRD	X-ray diffraction
XRF	X-ray fluorescence

aftertreatment catalysts may be especially challenging, because of the small amounts volatilised [3,7–9]. The few studies currently available have used oxidation or hydrogenation tests to test for the presence of noble metal traces, since the limit of detection of conventional analysis methods is not low enough [7–9]. For instance, Jen et al. estimated 0.0005-0.001 wt.% Pt in a contaminated SCR catalyst, so X-Ray Fluorescence (XRF) with a 0.002 wt.% detection limit was not sufficient [9]. Inductive Coupled Plasma – Mass spectrometry (ICP-MS) methods have been shown to be the most useful and robust in quantifying ultra-traces of noble metals [3].

A few articles in the published literature explored the concern of noble metal poisoning. These have focussed on understanding the impact of the presence of noble metals on SCR catalysts, typically via impregnation of the noble metal [10,11]. Some studies of the actual poisoning process through volatilisation used commercial DOC catalysts and/or engine bench tests to probe the extent of the deactivation of the SCR catalyst [2,7–9]. However, commercial catalysts are very complex and can include several unknown components, which makes analysis more difficult. For instance, Cavataio et al. found contradictory results from two commercial DOC catalysts with the same Pt:Pd ratio, and so could not conclusively determine the impact of Pd content on Pt-containing DOCs [8]. Carrillo et al. [20] conducted a fundamental study regarding Pt volatilisation and sintering from Pt-Pd/SiO_2 materials. In this work the noble metals were evaporated on silicon wafer model TEM grids and studied with electron probe microanalysis (EPMA) and it was found that Pd lowered the emission of Pt.

However, there are to our knowledge no studies available that examine the noble metal volatilisation from well characterised model DOC monoliths. Nor is it known how the volatilised PGMs deposit, change their behaviour over time, or are affected by the oxidation tests used to test for their presence. Our goal in this study is therefore to examine the way noble metals volatilise and deposit from well-characterised Pt and/or Pd-containing model DOCs, supported on Al_2O_3 in function of various operating parameters, such as temperature, duration, atmospheric composition and catalyst Pd content.

2. Experimental methods

2.1. Catalyst preparation

Both Pt/Al_2O_3 and Pd-Pt/Al_2O_3 with different Pd concentrations were produced via incipient wetness impregnation of alumina (Sasol Puralox Nga150). The pore volume of the material was obtained by N_2 physisorption and was 0.524 mL/g. This allowed for calculation of the amount of precursor necessary to impregnate the alumina support to achieve the desired Pt content of 2 wt%. The Pt precursor used was a diamminedinitritoplatinum (II) solution (3.4 wt% in NH_4OH) from Sigma Aldrich.

For the preparation of Pt/ Al_2O_3, a two-step impregnation procedure was required. In each step, the precursor was dissolved in MiliQ water, producing a solution with the exact volume necessary to completely fill the pores of the alumina support. Between the steps, the material was dried at 100 °C for 19 h. Once the second step of impregnation was completed, the material was calcined in a furnace at 500 °C for 2 h with a ramp of 5 °C/min. Two batches of Pt/Al_2O_3 were produced.

Likewise, for the preparation of Pd-Pt/Al_2O_3, a stepwise procedure was employed. First, the overall procedure described for the production of Pt/Al_2O_3 was repeated, followed by a single-step impregnation with Pd, aiming for a Pd:Pt = 20:80 wt ratio. The precursor used here was a tetramminepalladium (II) nitrate solution (10 wt. % in H_2O from Sigma Aldrich). After Pd impregnation, the material was dried at 100 °C overnight. Calcination was then performed for 2 h at 500 °C, with a ramp of 5 °C/min. A part of the resulting catalyst (Pd:Pt = 0.5:1 mol/mol) was used for further Pd impregnation with the same precursor and the same procedure to obtain two higher Pd:Pt ratios, Pd:Pt = 1:1 mol/mol and Pd:Pt = 2:1 mol/mol.

A Pd/Al_2O_3 catalyst was also prepared, following a one-step impregnation procedure and using the same tetramminepalladium (II) nitrate precursor. The aim was to produce a catalyst with the same number of moles of noble metal as in the Pt/Al_2O_3 catalysts. After Pd impregnation, the material was dried at 100 °C overnight. Calcination was then performed for 2 h at 500 °C, with a ramp of 5 °C/min.

Inductively Coupled Plasma – Sector Field Mass Spectrometry (ICP-SFMS) analysis showed that the Pt content of the two Pt/Al_2O_3 catalysts was similar, and close to the 2 wt% target value, at 1.99 and 1.88 wt%. The Pd-Pt/ Al_2O_3 catalysts contained a similar amount of Pt and 0. 49, 0.95 and 1.85 wt% Pd for the Pd:Pt = 0.5:1, 1:1 and 2:1 respectively. The Pd/Al_2O_3 catalyst contained 1.05 wt% Pd. Further compositional details are given in Table 1. Note that some of the analyses were repeated, in those cases the given value is an average. Both values are given in Table S1 in the Supplementary Material. Some analyses were also conducted on the commercial DOC, with the details shown in Table 1.

The supported noble metal catalysts were washcoated on monolith cores cut from commercial honeycomb cordierite. Length of the cores was 20 mm, diameter 15 mm and channel density 400 cpsi, with a total of 89 channels per monolith. Prior to washcoating, the cores were all calcined in air at 500 °C for 2 h. Approximately 250 mg washcoat, consisting of 95 wt% catalyst + 5 wt% boehmite binder (Disperal P2),

Table 1
Elemental composition (from ICP-SFMS) of catalysts used in the study. n.a. – not analysed.

	Pd (wt%)	Pt (wt%)	Rh (wt%)	Pd (mol/g_{tot})	Pt (mol/g_{tot})
Pt/Al_2O_3 Batch 1	$9.37{\cdot}10^{-5}$	1.99	$< 3.00{\cdot}10^{-5}$	$8.80{\cdot}10^{-9}$	$1.02{\cdot}10^{-4}$
Pt/Al_2O_3 Batch 2	$7.47{\cdot}10^{-3}$	1.88	$< 3.00{\cdot}10^{-5}$	$7.01{\cdot}10^{-7}$	$9.64{\cdot}10^{-5}$
Pd-Pt/Al_2O_3(Pd:Pt = 0.5:1)	0.49	1.90	$< 3.00{\cdot}10^{-5}$	$4.55{\cdot}10^{-5}$	$9.71{\cdot}10^{-5}$
Pt/Al_2O_3(Pd:Pt = 1:1)	0.95	1.79	$< 3.00{\cdot}10^{-5}$	$8.92{\cdot}10^{-5}$	$9.18{\cdot}10^{-5}$
Pt/Al_2O_3(Pd:Pt = 2:1)	1.85	1.78	$< 3.00{\cdot}10^{-5}$	$1.74{\cdot}10^{-4}$	$9.12{\cdot}10^{-5}$
Pd/Al_2O_3	1.05	$< 5.00{\cdot}10^{-4}$	$< 5.00{\cdot}10^{-4}$	$9.87{\cdot}10^{-5}$	$< 2.6{\cdot}10^{-8}$
Commercial DOC	0.09	0.50	n.a.	$8.42{\cdot}10^{-6}$	$2.56{\cdot}10^{-5}$

was coated onto each core. This was done by repeated dipping in a slurry consisting of 95% liquid phase (equal parts deionized water and ethanol) and 5% solid phase. After each dipping, excess slurry was blown away and the core dried for several minutes at 90 °C. When the desired washcoat mass had been obtained, the core was calcined in air at 500 °C for 2 h. These monolith cores are referred to as "parent monoliths". Further, an equal number of cores was washcoated with ca. 70 mg Disperal P2 each, and calcined under the same conditions. These are referred to as "capturing monoliths". Details on the washcoated amounts for both parent and capturing monoliths are provided in Table S1, see Supplementary Material. Note that the commercial DOC catalyst was provided already washcoated on a large honeycomb, from which small cores were cut, of the same size as the noble metal parent monoliths. These small cores were also calcined in air at 500 °C for 2 h before used in experiments.

2.2. Vaporisation experiments

All the vaporisation experiments were performed using the washcoated monoliths in a flow reactor. A noble metal-washcoated parent monolith was inserted in a horizontal quartz tube, and approximately 12 cm downstream of it, an alumina-coated capturing monolith was placed. A schematic of this setup is shown in Fig. 1. The reason for using alumina coating on the capturing monolith was the need for a material that is inert for ammonia oxidation, has high surface area and is stable at high temperatures. In this way we could determine the ammonia oxidation activity for the deposited platinum. The monoliths were wrapped in quartz wool to prevent gas slip and the quartz tube was 70 cm long, with an internal diameter of 16 mm. Three K-type thermocouples were inserted into the reactor through a Teflon ferrule, and were positioned with their tips respectively five mm upstream of the parent monolith, in the centre of the parent monolith, and in the centre of the capturing monolith. The former two thermocouples provided a measurement of the gas phase temperature and the temperature of the supported noble metal catalyst. These measurements were recorded continuously in LabView. The third thermocouple measured the temperature of the alumina-coated capturing monolith, and the temperature was displayed on a separate terminal and recorded once towards the end of the experiment.

The reactive gas mixture at the inlet to the reactor (Ar as balance, O_2 and water vapour), was regulated using Bronkhorst massflow controllers and water vapour was produced by a controlled evaporation and mixing (CEM) system (Bronkorst). The reactor temperature was controlled by a heating unit consisting of a Eurotherm controller, a heating coil placed around the reactor tube and a power supply. The heating coil was so positioned as to include the noble metal parent monolith as shown in Fig. 1. Thus the temperature in the parent monolith, and that of the gas immediately upstream of the parent monolith, could be controlled. Additionally, the reactor tube was wrapped in insulating wool in order to maintain the set temperature in the parent monolith. The temperature in the capturing monolith was on average around 350 °C, but the exact value depended on the temperature of the parent monolith since the distance between the parent and capturing monoliths was kept fixed. All temperatures in the experiments can be found in Table 2. All lines upstream and downstream of the reactor were heated to 150 or 200 °C to prevent condensation of water vapour. The reactor was operated at a total flow rate of 1200 ml/min, corresponding to a gas hourly space velocity (GHSV) of 23,390 h^{-1} (0 °C, 1 atm), on the basis of the volume of a single monolith (capturing and parent monoliths have the same volume).

Prior to the vaporisation experiment, a lean pre-treatment step and a degreening step were run, with both parent and capturing monoliths already in their positions inside the reactor. The degreening consisted of lean pretreatment for 20 min at 500 °C in presence of 300 ppm C_3H_6, 8% O_2 and 5% H_2O, followed by 400 ppm NO, 8% O_2 and 5% H_2O for 3 h at 500 °C, to ensure stable activity. The volatilisation step itself had different durations and target temperature in each experiment, as may be seen in Table 2. Gas composition during the volatilisation was 8% O_2 and 5% H_2O in Ar, unless otherwise mentioned. In total, data from 48 such experiments is included in this study, and all these experiments are listed in Tables 2 and S2. For the case of parent core P14, four consecutive vaporisation experiments were performed at different temperatures, each with a new capturing core. For the second, third and fourth vaporisation experiments with P14, no degreening/pretreatment step was performed. Note that some experiments were not included in the text or Table 2 because the temperature gradient between the gas phase and the parent monolith was larger than 30 °C, and thus the value of the parent core temperature over the monolith length was uncertain.

2.3. Catalyst characterisation

2.3.1. Capturing monoliths

After the vaporisation experiments, the capturing monoliths were analysed for NH_3 and CO oxidation activity, as a measure of the presence of captured noble metal. The monolith was placed in another reactor setup similar to that described in Section 2.2 and also using Ar as the carrier gas. Only two thermocouples were present in this setup, allowing for continuous measurement of the surface temperature in the centre of the capturing monolith, and of the gas five mm upstream of the monolith. The fractions of the outlet gases, NH_3, NO, NO_2, N_2O, CO and H_2O, were measured at the outlet of the reactor by a MKS™ Multigas 2030 FTIR spectrometer.

Each of the capturing monoliths analysed for oxidation ability was thus subjected to the following sequence of pre-treatments and activity experiments, all performed with a total flow rate of 1200 ml/min (corresponding to a gas hourly space velocity (GHSV) of 23,390 h^{-1}, on the basis of the volume of a single capturing monolith).

- O_2 pre-treatment: 8% O_2, 5% H_2O, 20 min, 500 °C
- NH_3 oxidation n1: 400 ppm NH_3, 8% O_2, 5% H_2O, 10 °C/min from 100 °C to 500 °C
- O_2 pre-treatment: 8% O_2, 5% H_2O, 20 min, 500 °C
- CO oxidation n1: 400 ppm CO, 8% O_2, 5% H_2O, 10 °C/min from 100 °C to 500 °C
- O_2 pre-treatment: 8% O_2, 5% H_2O, 20 min, 500 °C
- NH_3 oxidation n2: 400 ppm NH_3, 8% O_2, 5% H_2O, 10 °C/min from 100 °C to 500 °C
- O_2 pre-treatment: 8% O_2, 5% H_2O, 20 min, 500 °C

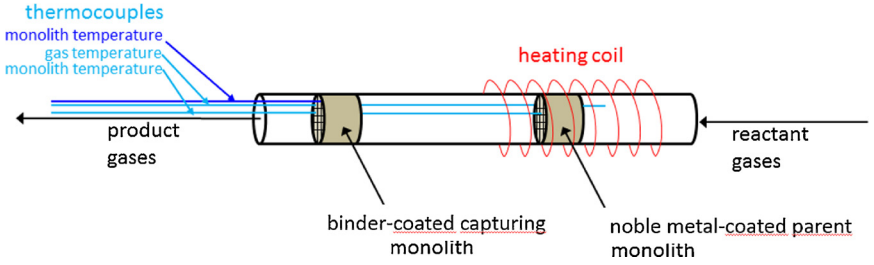

Fig. 1. Schematic of the reactor setup used for vaporisation experiments.

Table 2
List of all vaporisation experiments performed in this study, with relevant experimental conditions. Note that experiments with the commercial DOC are not listed here, but in Table S2. nm - not measured.

Exp. no.	Gas temp. [°C]	Parent core temp. [°C]	Capturing core temp. [°C]	Vapor. duration [h]	Feed gas	Parent catalyst	Parent core no.	Capturing core no.
1	550	536	233	15	8% O_2, 5% H_2O	Pt	P1	C1
2	550	542	262	15	8% O_2, 5% H_2O	Pd	P2	C2
3	550	543	269	15	8% O_2, 5% H_2O	Pd:Pt = 0.5:1	P3	C3
4	700	692	nm	5	8% O_2, 5% H_2O	Pd:Pt = 0.5:1	P4	C4
5	700	695	388	5	8% O_2, 5% H_2O	Pt	P5	C5
6	700	686	360	10	8% O_2, 5% H_2O	Pt	P6	C6
7	700	690	334	15	8% O_2	Pt	P7	C7
8	700	679	333	15	Ar	Pt	P8	C8
9	700	729	312	15	Ar	Pt	P9	C9
10	700	679	329	15	8% O_2, 5% H_2O	Pd	P10	C10
11	700	693	279	15	2% O_2, 5% H_2O	Pt/Al_2O	P11	C11
12	700	693	301	15	5% O_2, 5% H_2O	Pt/Al_2O	P12	C12
13	700	683	301	15	8% O_2, 5% H_2O	Pt	P13	C13
14	700	684	332	15	8% O_2, 5% H_2O	Pt	P14	C14
15	700	685	327	15	8% O_2, 5% H_2O	Pt	P15	C15
16	700	685	318	15	8% O_2, 5% H_2O	Pd:Pt = 0.5:1	P16	C16
17	700	686	330	15	8% O_2, 5% H_2O	Pt	P17	C17
18	700	686	300	15	8% O_2, 5% H_2O	Pd:Pt = 0.5:1	P18	C18
19	700	691	337	15	8% O_2, 5% H_2O	Pt	P19	C19
20	700	695	384	15	8% O_2, 5% H_2O	Pt	p20	C20
21	700	685	321	30	8% O_2, 5% H_2O	Pt	P21	C21
22	700	677	328	35	8% O_2, 5% H_2O	Pt	P22	C22
23	700	678	337	35	8% O_2, 5% H_2O	Pd:Pt = 0.5:1	P23	C23
24	700	692	nm	40	8% O_2, 5% H_2O	Pt	P24	C24
25	700	693	340	40	8% O_2, 5% H_2O	Pt	P25	C25
26	700	699	371	40	8% O_2, 5% H_2O	Pd:Pt = 0.5:1	P26	C26
27	700	nm	311	40	8% O_2, 5% H_2O	Pt	P27	C27
28	780	756	355	15	Ar	Pt	P28	C28
29	780	746	369	15	8% O_2, 5% H_2O	Pd:Pt = 0.5:1	P29	C29
30	780	759	nm	15	8% O_2, 5% H_2O	Pt	P30	C30
31	850	811	392	15	8% O_2, 5% H_2O	Pd:Pt = 0.5:1	P31	C31
32	850	824	384	15	8% O_2, 5% H_2O	Pd	P32	C32
33	850	829	424	15	8% O_2, 5% H_2O	Pt	P33	C33
34	850	833	368	15	8% O_2, 5% H_2O	Pt	P34	C34
35	850	835	404	15	8% O_2, 5% H_2O	Pd:Pt = 0.5:1	P35	C35
36	850	837	373	15	8% O_2, 5% H_2O	Pt	P36	C36
37	700	689	324	15	8% O_2, 5% H_2O	Pd:Pt = 1:1	P37	C37
38	780	768	400	15	8% O_2, 5% H_2O	Pd:Pt = 1:1	P38	C38
39	850	820	402	15	8% O_2, 5% H_2O	Pd:Pt = 1:1	P39	C39
40	850	836	364	15	8% O_2, 5% H_2O	Pd:Pt = 1:1	P40	C40
41	780	761	365	15	8% O_2, 5% H_2O	Pd:Pt = 2:1	P41	C41
42	850	833	400	15	8% O_2, 5% H_2O	Pd:Pt = 2:1	P42	C42
43	850	837	385	15	8% O_2, 5% H_2O	Pt	P14	C43
44	780	760	363	15	8% O_2, 5% H_2O	Pt	P14	C44
45	700	679	292	15	8% O_2, 5% H_2O	Pt	P14	C45

- CO oxidation n2: 400 ppm CO, 8% O_2, 5% H_2O, 10 °C/min from 100 °C to 500 °C

In this paper only the second NH_3 oxidation experiment (n2 in the sequence above) is analysed, with the exception of Section 3.2 where the results from all oxidations, for certain monoliths, are evaluated for insight on the state of the captured Pt species. Two samples were subjected to six repeated NH_3 and CO oxidations, respectively, instead of the sequence above, also with the same O_2 pre-treatment before each experiment. These results are also discussed in Section 3.2. The temperature at which 50% or 20% of the NH_3 or CO was oxidised, was determined and used for comparison of the capturing monoliths. It is hereafter referred to as T_{50} or T_{20}.

After oxidation activity experiments, the capturing monoliths were crushed and ICP-SFMS was used to determine the elemental composition, with the aim of determining how much noble metal had vaporised and been captured by the capturing monolith. The measurements were carried out by ALS Scandinavia AB. The obtained weight composition was used to calculate the number of moles of noble metal deposited on each monolith. Limit of detection of the ICP-SFMS method was 0.3 or 0.5 mg/kg, depending on the mass of sample analysed. For a few cases, the amount of platinum was below the detection limit and for these cases this is clearly noted in the caption of the Figure. Note that the captured amounts of noble metal are very small, and hence other analysis techniques such as XRF cannot be used [9]. ICP-MS methods are known to be the most appropriate to analyse ultra-traces of noble metals, for example in environmental samples [3]. Also note that ICP-SFMS was likewise used to determine composition of the pure catalyst powders before washcoating.

Moreover, the amount of Pt deposited downstream of the capturing core is minor. For two earlier experiments (with slightly different pre-treatment conditions) we analysed inlet and outlet of the capturing core separately by ICP-SFMS, and found a significant difference in the Pt concentration: For one such core, Pt wt% was $1.3{\cdot}10^{-4}$ wt% at the inlet of the core, and $4.8{\cdot}10^{-6}$ at the outlet of the core. Similarly, for another core, Pt wt% was $1.4{\cdot}10^{-3}$ wt% at the inlet of the core, and $7.4{\cdot}10^{-6}$ at the outlet of the core.

2.3.2. Parent monoliths

After the vaporisation experiment, a small amount of the supported noble metal washcoat was scraped off the parent monoliths and characterised by scanning transmission electron microscopy (STEM) and energy-dispersive X-ray spectroscopy (EDX). The instrument used was a FEI Titan 80–300 microscope equipped with a field emission gun (FEG),

a probe Cs corrector, and a Gatan image filter (GIF) Tridium, operating at 300 kV, equipped with EDX. The samples were prepared by making a suspension of the washcoat in ethanol and drying this on the carbon coated copper grid at room temperature. The obtained images were analysed semi-automatically using ImageJ for obtaining particle size distributions. A total of ca. 100–150 particles were measured for each sample. The particle diameter was obtained by determining the area of the best-fitting ellipse, and then calculating an equivalent diameter assuming circular particles. EDX mapping was done in one spot (over large particles of 20–50 nm) for three Pd-Pt/Al_2O_3 (Pd:Pt = 0.5:1) samples.

Thereafter the parent monoliths were crushed, finely ground and then characterised using N_2 physisorption, X-ray diffraction (XRD) and diffuse reflectance infrared spectroscopy (DRIFTS). Nitrogen adsorption-desorption at 77 K for Brunauer-Emmett-Teller (BET) measurements and t-plot pore volume measurements was performed using a Tristar 3000 (Micromeritics) instrument. Prior to the measurement, the samples were outgassed under vacuum at 200 °C for 3 h. The X-ray diffractograms were obtained using a Bruker AXS D8 advance operating at 40 kV and 40 mA with nickel-filtered Cu Kα radiation (λ = 1.5418 Å) in the range $5^\circ < 2\theta < 40^\circ$ with a step size of 0.028°. DRIFTS measurements were performed using a Bruker 70 FTIR spectrometer and Harrick Praying Mantis DR accessory connected to a gas flow system with Bronkhorst mass flow controllers, similar to that described in Section 2.1.1. Approximately 70 mg of crushed parent monolith powder was placed on a porous grid in the sample cup. The sample was covered by a dome equipped with two KBr windows, and reactant gases were flown through the sample. Each sample was pretreated for 60 min in 2% H_2 at 500 °C and then cooled down to 30 °C. At this temperature a background was first acquired under Ar flow, and then the flow was switched to 1% CO for 30 min. During this time, a spectrum was acquired every 60 s using a scanner velocity of 20 kHz and a resolution of 4 cm^{-1}.

3. Results and discussion

3.1. Noble metal volatilisation from a commercial DOC

The basis of this study are the vaporisation experiments listed in Tables 2 and S2, where a noble metal catalyst-coated monolith is placed upstream of an alumina-coated monolith and a heated gas flow is streamed through the two monoliths, see Fig. 1. These experiments model the situation occurring in an automotive exhaust aftertreatment system when a DOC or a coated DPF is positioned upstream of an SCR component, leading to the volatilisation of noble metals from the high-temperature DOC. The volatilised noble metal can subsequently deposit on the SCR catalyst [9]. Note that this study was done on a flow through system of parent and capturing monolith. In many real aftertreatment systems, there is a filter in between and a long decomposition tube that partly mitigates the concern of Pt poisoning even if DOCs are exposure to high temperatures. Fig. 2a summarises the results of vaporisation experiments performed at different temperatures, using a commercial DOC catalyst. There is clearly a movement of small amounts of platinum from the parent monolith to the capturing monolith. Moreover, since an increasing trend with temperature is evident, the platinum must have volatilised prior to gas-phase transport, rather than being caused by simple blowing away of loosely washcoated catalyst powder. Jen et al. also ruled out blown-away powder in similar experiments, by packing quartz wool between a DOC and SCR catalyst [9]. We also rule out that significant amounts of platinum move through the capturing monolith without depositing, as in two early experiments, inlet and outlet of the capturing monolith were analysed separately, and it was found that the Pt content of the inlet was at least an order of magnitude higher (see Section 2.3.1), as also found by Chen et al. [7]. The capturing monoliths were also analysed for Pd and Rh, but both elements were found to be below detection limit (0.3 or 0.5 mg/kg, depending on the amount of sample and digestion method employed).

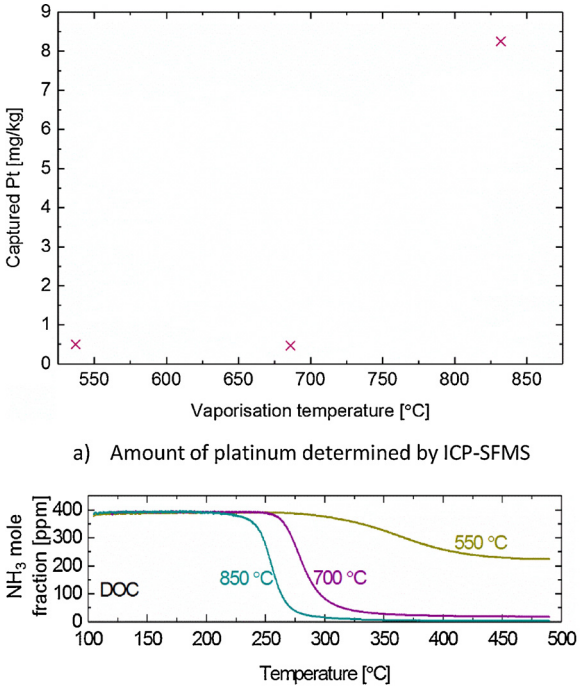

Fig. 2. Effect of vaporisation temperature on the amount of platinum deposited on a capturing monolith positioned downstream of a commercial DOC, as determined by ICP-SFMS and NH_3 oxidation. Vaporisation with 8% O_2, 5% H_2O, 15 h, 1200 ml/min, SV = 23,390 h^{-1}. Note that in a) the point at 550 °C corresponds to ICP-SFMS detection limit.

We tried to further characterise the capturing monoliths using STEM as well as *in-situ* DRIFT spectroscopy and CO chemisorption, but it was not possible to detect such small amounts of platinum. We therefore chose to test for the presence of platinum with another method. Even trace amounts of noble metals are known to be highly active for the oxidation of ammonia and carbon monoxide, and thus the sequence of two consecutive, temperature-programmed NH_3 and CO oxidation tests described in Section 2.1.1 was performed on each capturing monolith before ICP-SFMS analysis [9]. We tested for ammonia oxidation ability, because it is precisely this ability which is the cause of the unwanted deactivation of the downstream SCR catalyst, and therefore we seek to understand how ammonia oxidation proceeds over a noble-metal poisoned catalyst. The oxidation behaviour of the downstram core (representing an SCR component in a real system) is critical for understanding changes over time in the severity of noble metal poisoning. The reason that we used only alumina on the capturing monolith was to isolate the ammonia oxidation activity from the deposited platinum only, without interference of ammonia oxidation over the SCR material. The results of the second NH_3 oxidation test performed on the capturing monoliths placed downstream of the commercial DOCs are shown in Fig. 2b. It is immediately apparent that the amount of ammonia consumed follows the same trend to the amount of Pt determined by elemental analysis, i.e., increasing with vaporisation temperature. Note also that the activity for ammonia oxidation is significant, so that an SCR catalyst functioning as a "capturing monolith" would have been severely deactivated by competitive ammonia consumption. It was further verified that the ammonia oxidation ability of the capturing monolith did indeed originate during the vaporisation experiment, and not by some earlier contamination, by subjecting a "fresh" capturing monolith that had undergone no vaporisation experiment, to the oxidation test sequence. The "fresh" capturing monolith showed no NH_3 and CO oxidation ability, which is consistent with the known fact that γ-alumina is inactive for NH_3 oxidation [21].

3.2. Stability of the deposited platinum species on capturing monoliths

Vaporisation experiments were performed at different temperatures on commercial DOC, Pt/Al_2O_3 and $Pd\text{-}Pt/Al_2O_3$ catalysts. Before discussing the trend with vaporisation temperature in Section 3.3, however, we here examine the stability of the deposited platinum, and the implications of platinum restructuring for interpretation of the ammonia oxidation experiments. This investigation is of interest not only because it aids in interpretation of the ammonia oxidation tests as indicators of volatilised amounts, but also because the behaviour of deposited Pt over time is crucial in the deactivation of a contaminated downstream SCR catalyst. Ammonia oxidation experiments number 1 and 2 are shown in Fig. 3a for nine different capturing monolith samples. Similarly, CO oxidation experiments number 1 and 2 are shown in Fig. 3b. The first oxidation experiment is indicated by a solid line, the second by a dashed line. For NH_3 oxidation, it can be seen that for six out of the nine samples, there is a significant difference between the first and the second test and the activity of the second test is larger than that of the first test. For CO oxidation, on the other hand, the difference is quite small, and in most cases, negligible. It should be noted that the order of the experiments was NH_3 oxidation No.1, CO oxidation No. 1, NH_3 oxidation No.2 and CO oxidation No. 2. Thus, prior to the first CO oxidation experiment there was an ammonia oxidation experiment.

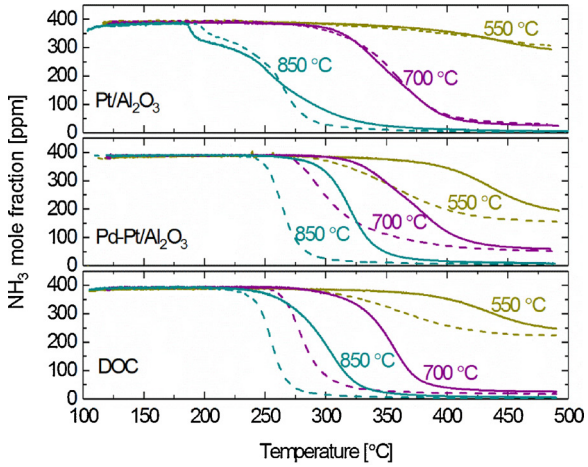

a) NH_3 oxidation: SV=23390 h^{-1}

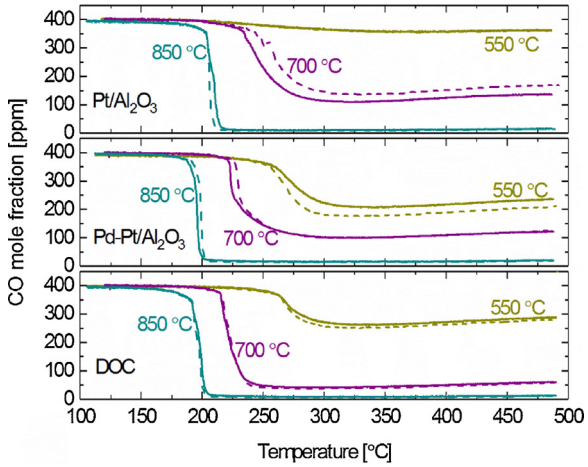

b) CO oxidation: SV=23390 h^{-1}

Fig. 3. Change in oxidation ability of capturing monoliths upon repetition: oxidation n.1 (solid line) vs n.2 (dashed line) of the oxidation sequence. Vaporisation of Pt/Al_2O_3, $Pd\text{-}Pt/Al_2O_3$ and commercial DOC with 8% O_2, 5% H_2O, 15 h, 1200 ml/min, SV = 23,390 h^{-1} at different temperatures.

It is well known that the oxidation reactions are sensitive to the surface structure of platinum catalysts [22–28]. Particularly relevant for supported platinum catalysts is the observation that ammonia oxidation activity increases with increasing particle size [24–26,29]. We therefore propose that the change in oxidation ability here is brought on by a change in the structure by clustering of Pt atoms occurring during repeated experiments and pre-treatments. The deposited platinum is probably dispersed very finely, or even on atom level, since it is formed by volatile platinum species and thereafter sinters in the experiment. Given the very small amounts of platinum deposited on the capturing monolith, it was not possible to examine the structure of the platinum surface using high resolution TEM, nor were we able to determine the dispersion of platinum particles by means of CO titration. However, on the basis of what is known from literature, conclusions can be made from the changing NH_3 and CO oxidation abilities.

In order to find out whether the reason for observing only minor effects in the CO oxidation activity was that it was conducted after the NH_3 oxidation experiment, we conducted new experiments subjecting the capturing monoliths to either six successive NH_3 oxidations or six successive CO oxidations, as shown in Fig. S1a and e (Supplementary material). The corresponding NO, N_2O and NO_2 concentrations of the NH_3 oxidation experiments are also shown in the same Fig. (S1 b–d). As expected, there was a large difference between the first and second ammonia oxidation tests, but the difference between the following experiments was small. This observation supports the interpretation that most of the particle size increase occurs during the first oxidation experiment. Like the NH_3 oxidations, the CO oxidation activity in Fig. S1e also undergoes an increase after the first test, and is thereafter stable.

In summary, the Pt-poisoned monoliths show considerable NH_3 and CO oxidation ability, but this ability depends significantly on the surface structure of the deposited Pt. Exposure to a reactive atmosphere at temperatures up to 500 °C causes the oxidation ability to increase, likely because of an increase in Pt particle size. This is significant for Pt-poisoning occurring in a real exhaust aftertreatment system, since it means that the poisoning effect of parasitic NH_3 consumption will change over time and depending on the conditions in the poisoned SCR component. Regarding our use of these experiments here as indicators of amount of volatilisation, we focus on the second oxidation test in the following sections, because the change in oxidation ability due to exposures subsequent to the second one is small.

3.3. Effect of vaporisation temperature on noble metal oxide volatilisation

The literature from a variety of different applications suggests that platinum oxides (PtO_x) are the main volatile species. However, given the wide variability that is observed with the very different systems in which volatilisation has been studied, we performed volatilisation experiments with different O_2 and H_2O concentrations, to confirm that PtO_x are indeed the volatilising species in a model exhaust aftertreatment system. Our findings and the relevant literature are discussed in the Supplementary Materials. In brief, the results confirm that deposition of platinum on a monolith downstream from a model DOC (Pt only) in the vaporisation temperature range 550–850 °C occurs primarily via the volatile platinum oxides.

In order to study the effect of temperature, vaporisation experiments of duration 15 h and with 5% H_2O and 8% O_2 were performed at several different temperatures between 550 and 850 °C for Pt/Al_2O_3, $Pd\text{-}Pt/Al_2O_3$ of three different Pd:Pt ratios and Pd/Al_2O_3-coated cores. In this section, volatilisation from the platinum-only catalysts will be discussed; the effect of Pd will be discussed in a later section. Amounts of platinum deposited on the downstream capturing monolith were obtained by ICP-SFMS analysis of the crushed capturing monoliths, and are plotted in Fig. 4a as a function of the vaporisation temperature. The capturing cores were also analysed for traces of Pd, but the value was close to or below detection limit for all samples.

Overall, Pt volatilisation from Pt/Al_2O_3 increases with temperature,

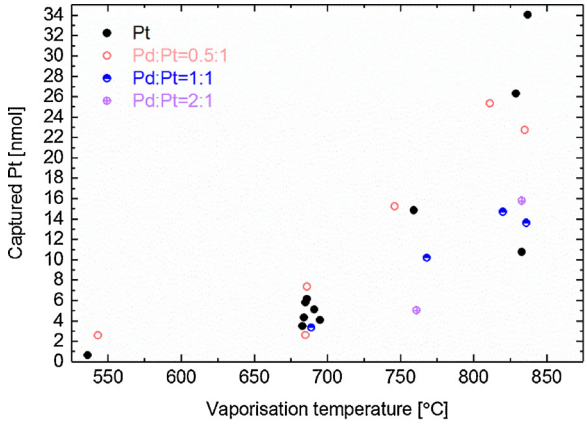

a) Amount of deposited Pt, as determined by ICP-SFMS.

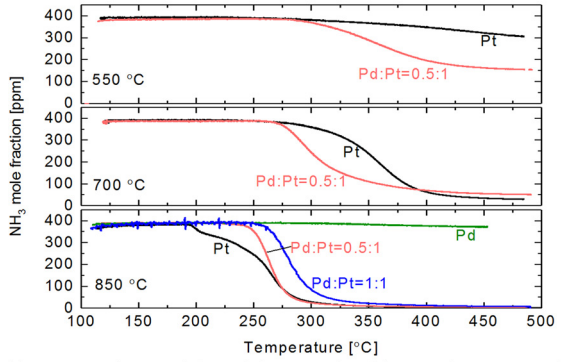

b) NH_3 oxidation ability of deposited noble metal. SV=23390 h^{-1}.

Fig. 4. Effect of vaporisation temperature on the amount of platinum deposited on a capturing monolith positioned downstream of Pt/Al_2O_3 and Pd-Pt/Al_2O_3 monoliths, as determined by ICP-SFMS and NH_3 oxidation. Vaporisation with 8% O_2, 5% H_2O, 15 h, 1200 ml/min, SV = 23,390 h^{-1}. Note that in a) the point for Pd-Pt (Pd:Pt = 0.5:1) at 550 °C and the lower point at 700 °C correspond to ICP-SFMS detection limit.

except for one point at around 830 °C, which does not fit into the apparent trend. The difference between this point and other points at around 830 °C is too large to be accounted for by the normal variability seen for several repeated experiments around 700 °C. We believe that this point is an outlier, and caused by a variation in one of the experimental parameters, several of which are very difficult to control precisely (distance between monoliths, temperature on the capturing monolith, dispersion of the synthesised catalyst etc.). To test this assumption, we performed linear and exponential fits on both the whole data set, and the data set without the suspected outlier point, as shown in Fig. 5. In both cases, the exponential fit was better, and when removing the suspected outlier, the fit became very good, with an R^2 coefficient of 0.97, as opposed to the linear fit with 0.56. An exponential trend with temperature is expected. Alcock and Hooper, Schäfer, Jehn and others found exponential trends for PtO_2 vapour pressures or Pt mass loss from platinum discs, wires and gauzes exposed to O_2 flows [12–14,30,31]. Moreover, platinum oxide formation can be expected to follow an exponential Arrhenius law, and vaporisation processes are described by the exponential Clausius-Clapeyron law [12,32]. However, to the best of our knowledge, no such data have been published for supported Pt catalysts. The exponential fit to the data without the outlier point can be written as $\ln(n_{Pt}) = 99/(RT) + 14$, in the form of the Clausius-Clapeyron equation. The slope (99/R) is smaller than that obtained by Alcock and Hooper and Schäfer for measured vapour pressures, ~170/R, where 170 kJ/mol is the enthalpy of vaporisation. This could speculatively be attributed to the fact that we examined Pt particles supported on Al_2O_3 and the aforementioned authors used pure Pt wires [30,33], which could affect the evaporation process.

The trend for ammonia oxidation activity of deposited platinum over the capturing monolith is also increasing with vaporisation temperature, as can be seen in Fig. 4b. Since 50% conversion is not reached for the sample tested at 500 °C, we calculated T_{20}, and its value is 465, 328 and 229 °C for vaporisation temperatures of 550, 700 and 850 °C, respectively. Both the trend for ammonia oxidation ability and the amount of deposited Pt clearly show a monotonic increase of vaporised platinum between the vaporisation temperatures of 550 and 850 °C. NO, N_2O and NO_2 production for the ammonia oxidation tests are shown in Fig. S3. NO selectivity is not greatly affected by the vaporisation temperature: in all cases the production of NO starts around 250–275 °C and reaches about 70–80 % at 500 °C. N_2O and NO_2 production remain similar going from T_{vap} = 550 °C to 700 °C, but undergo a noticeable increase for T_{vap} = 850 °C. This indicates that larger quantities of deposited Pt are necessary before NO is oxidised to NO_2 [7].

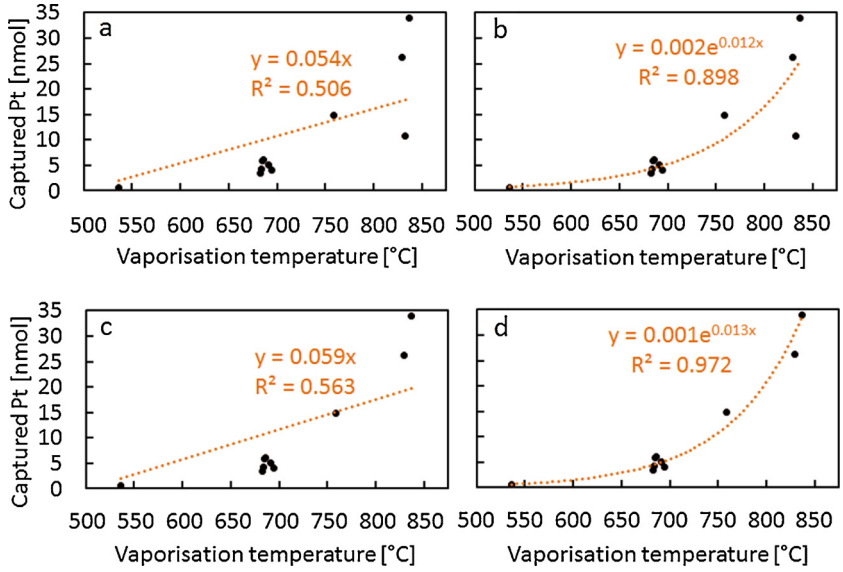

Fig. 5. Different fits of amounts of platinum deposited on a capturing monolith positioned downstream of Pt/Al_2O_3, in function of vaporisation temperature a and b are fits to all points, c and d are fits without the outlier point.

Table 3
BET surface areas (in m^2/g catalyst) of Pt/Al_2O_3 and $Pd\text{-}Pt/Al_2O_3$ (Pd:Pt = 0.5:1) after vaporisation experiments at different temperatures and with 8% O_2, 5% H_2O, 15 h, 1200 ml/min.

T_{vap} [°C]	Pt/Al_2O_3	$Pd\text{-}Pt/Al_2O_3$ (Pd:Pt = 0.5:1)
550	121	131
700	117	129
780	111	115
850	98	97

It is well-known that exposure of Pt/Al_2O_3 to high temperatures causes transformation of γ-alumina to lower-surface area aluminas, in the process encapsulating Pt particles inside closed-off pores [34,35]. This could well have an impact on the amount of Pt that is able to volatilise, so to examine this, we measured the BET surface area of the crushed parent monoliths (washoated with Pt/Al_2O_3) after vaporisation experiments at the different temperatures. The results are shown in Table 3. Surface area does decrease somewhat, to 81 and 74% of its original value for Pt and Pd-Pt catalysts, respectively. However, this decrease does not appear to have any effect on the volatilised amounts, since the latter follow the expected exponential trend with temperature.

Another factor that could be expected to have an effect on the vaporisation from supported noble metal catalysts is sintering [2]. Volatile PtO_2 has been suggested to be implicated in the sintering process as a mobile species responsible for particle growth in a number of publications [36–40]. Moreover, it is possible that the platinum particle size influences the rate of Pt volatilisation. We thus assess the extent of sintering using XRD, DRIFTS, STEM and repeated volatilisation experiments (see Section 3.5) in order to see whether increased particle size affects volatilisation.

Pt/Al_2O_3 and $Pd\text{-}Pt/Al_2O_3$-coated parent monoliths were crushed and analysed by XRD. The diffractograms are shown in Fig. 6. $Pd\text{-}Pt/Al_2O_3$ will be discussed in the following section, here we focus on Pt/Al_2O_3. The most prominent signal is that of the cordierite monolith substrate, shown in grey in the figure. There are three areas where the signal differs from the cordierite signal, around 39, 67.5 and 81.8°. These are marked by the diamond symbol in Fig. 6a and are characteristic of Pt (111), (220) and (311) [41]. The signal between 66 and 68° further contains a contribution from the alumina support. The main observation from Fig. 6a is that height and area of the most prominent Pt peak (Pt (111) at 39°) increase with vaporisation temperature for Pt/Al_2O_3. This indicates that Pt crystallite sizes are increasing with temperature, which is evidence of sintering. Because of the high cordierite content, the peaks are too small to allow for accurate Scherrer crystallite size determination. However, it is clear that, as expected, sintering increases with vaporisation temperature in Pt/Al_2O_3. Further evidence for this sintering trend in Pt/Al_2O_3 is seen from CO-DRIFTS in Fig. S4. Note that the sample underwent an H_2 pre-treatment before DRIFTS measurements, since CO adsorption is facilitated by reduced Pt, whereas samples analysed by XRD (and TEM, see below) underwent no such treatment. Despite this difference in pretreatment, the trends observed are similar: The peak at 2069 cm^{-1} (fresh, pure catalyst), characteristic for linearly adsorbed CO on metallic Pt, shifts to lower wavenumbers for the washcoated catalysts exposed to different vaporisation temperatures. This could be caused by a number of factors, such as the nature of the adsorption site, surface orientation or particle size, but also the presence of different compounds and co-adsorbates, since the IR spectrum of adsorbed-CO is very sensitive to all of these and can thus differ significantly [42,43]. However, when comparing only the samples exposed to different vaporisation temperatures to each other, we observe a shift to higher wavenumbers (e.g. 2046 cm^{-1} vs 2053 cm^{-1} for 550 vs 700 °C) and a strong decrease of intensity with increasing vaporisation temperature (washcoated monolith, after vaporisation), which is indicative of increasing particle size [42–46].

Particle size distributions were determined from TEM micrographs

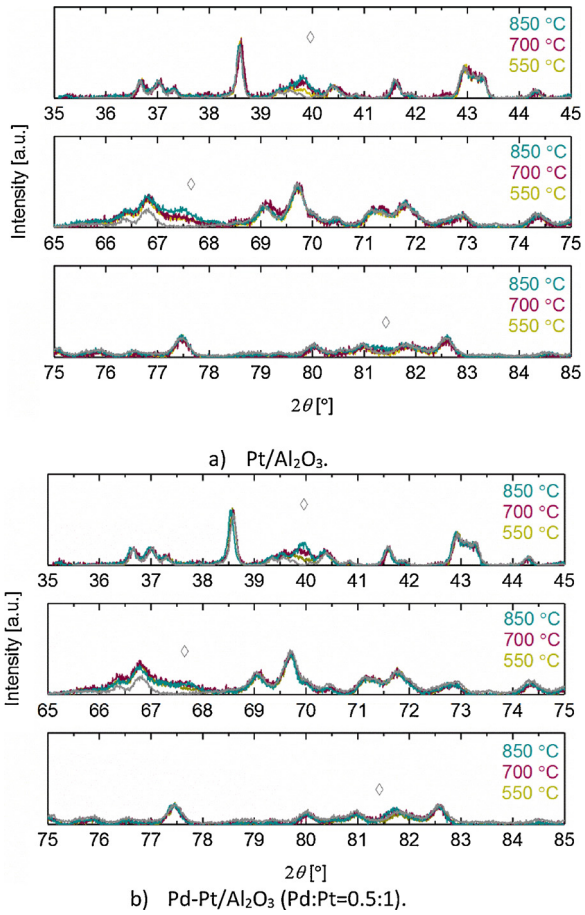

Fig. 6. X-ray diffractograms of noble metal parent monoliths after vaporisation experiments at different temperatures. Vaporisation with 8% O_2, 5% H_2O, 15 h, 1200 ml/min. Grey line – cordierite substrate. ◊ - Pt.

by counting roughly 100 particles per sample. The distributions for different vaporisation temperatures are shown in Fig. 7. Note that Fig. 7 does not show all observed particle sizes up to the maximum observed size, but is truncated at 40 nm for ease of visualisation. All particle size distributions are bimodal, with a majority of particles below 5 nm, and a second peak appearing centred above roughly 10 nm, although the smaller number of particles of this bigger size makes it difficult to determine the centre of the peak with accuracy in some of the distributions. The centre of the < 5 nm distribution of Pt/Al_2O_3 increases from roughly 1.5 nm for T_{vap} = 550 °C, to about 2.5 nm for T_{vap} = 850 °C. Similarly, the centre of the > 10 nm distribution increases from roughly 12 nm to roughly 20 nm. There also appears to be an increasing number of large (> 5 nm) particles with increasing vaporisation temperature. In summary, XRD, CO-DRIFTS and TEM all show that there is an increase of particle size with increasing temperature, in parallel with the increase in vaporisation.

Overall, both elemental analysis and ammonia oxidation activity tests showed that the amount of volatilised platinum oxide from a Pt/Al_2O_3 monolith increases with temperature. The increase is exponential, and, at least between evaporation temperatures of 550 and 850 °C, not significantly affected by sintering of the alumina support. Moreover, Pt particle size increased with increasing vaporisation temperature.

3.4. Effect of adding Pd to Pt/Al_2O_3 on volatilisation

In addition to the experiments with Pt/Al_2O_3 at different vaporisation temperatures, discussed in the previous section, similar experiments were also performed with $Pd\text{-}Pt/Al_2O_3$ and Pd/Al_2O_3-coated

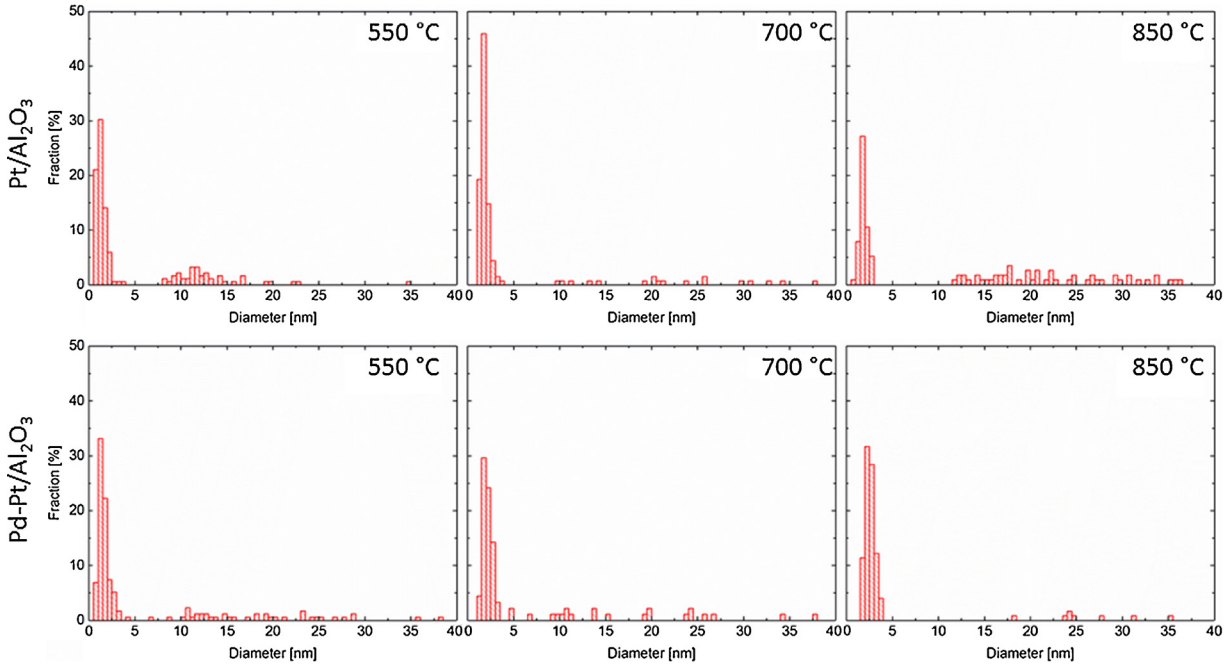

Fig. 7. Particle size distributions for noble metal parent monoliths after vaporisation experiments at different temperatures. Obtained by counting of particles in micrographs in Figure S5 and S6. Vaporisation with 8% O_2, 5% H_2O, 15 h, 1200 ml/min. For easier visualisation, the axis only shows diameters up to 40 nm, but maximum observed diameters for Pt and Pd-Pt (Pd:Pt = 0.5:1) at 850 °C are 50 and 74 nm.

cores for three different Pd:Pt ratios. Jen et al. found that noble metal poisoning of the downstream SCR catalyst was dependent on the formulation of commercial DOC catalysts [8,9]. It was also found that a Pd-only DOC caused no poisoning, but it was not clear whether this was due to little vaporisation of Pd, or due to low impact of volatilised Pd on the SCR catalyst. In addition, commercial DOC formulations with the same Pd:Pt ratio and total amount of noble metal loading caused significantly different levels of poisoning [8]. In order to understand these findings, we in this section examine the effect of increasing the Pd concentration and also examine Pd/Al_2O_3 as a reference. Amounts of platinum deposited on the downstream capturing monolith were obtained by ICP-SFMS analysis of the capturing monoliths, and are plotted in Fig. 4a as a function of the vaporisation temperature. The capturing monoliths were also analysed for Pd, but Pd was close to or below detection limit for all samples, even the Pd/Al_2O_3 catalyst and the commercial DOC (Fig. 2A). Hence, even in the Pd-Pt containing catalysts, the main species poisoning the downstream monolith are platinum-containing species. Clearly, for Pd-Pt/Al_2O_3 (Pd:Pt = 0.5:1), the trend of volatilised platinum oxides with temperature is very similar to that of the Pt/Al_2O_3 catalyst, i.e., exponential (Fig. 4a). Ammonia oxidation ability of the capturing monoliths also increases with temperature (Fig. 4b): The value of T_{20} is 340, 288 and 256 °C for vaporisation temperatures of 550, 700 and 850 °C, respectively. Note that also for the commercial DOC, ammonia oxidation ability is increasing with T_{vap} (Fig. 2a). The differences in selectivity (Fig. S3) between Pt/Al_2O_3 and Pd-Pt/Al_2O_3 (Pd:Pt = 0.5:1) are negligible, further confirming what was found by ICP-SFMS. Furthermore, ammonia oxidation ability is very small for a capturing monolith that had been placed downstream of a Pd-only catalyst at 850 °C, thus indicating that a very small amount of Pd volatilised, in accordance with ICP. It is likely that in the case of Pd, the poisoning species is Pd, and not PdO, since PdO is significantly less volatile [13,14,47]. However, the vapour pressure of Pd is still four orders of magnitude lower than that of PtO_2, (at 800 °C, 10^{-12} vs 10^{-8} atm) which explains why the amount of Pd poisoning is almost negligible compared to poisoning by PtO_2, even at 850 °C [14,47,48]. Finally, as with Pt/Al_2O_3, a decrease (26%) in BET surface area is seen for Pd:Pt = 0.5:1 (Table 3), but alumina sintering does not appear to significantly affect the volatilised amounts. While the trend of volatilised platinum oxides from Pd:Pt = 0.5:1, is indistinguishable from that of pure Pt, the catalysts with higher Pd:Pt ratios (1:1 and 2:1) present significantly less volatilisation, as seen in Fig. 4a.

EDX maps were obtained for the Pd-Pt/Al_2O_3 (Pd:Pt = 0.5:1) catalysts which had undergone vaporisation experiments at 550, 700 and 850 °C. The maps are presented in Fig. 8 and show large particles of roughly 20–50 nm in diameter. At all three temperatures, these large particles indicate Pd-Pt alloying, since the signals for Pt and Pd overlap inside of the particles. Despite evidence of alloying of the larger particles, we do not see any clear effect on the volatilised amounts upon addition of Pd to Pt/Al_2O_3, using a mol ratio Pd:Pt = 0.5:1. However, when adding larger amount of palladium to the Pd-Pt/Al_2O_3 (Pd/Pt: 1:1 and 2:1) the volatilisation is significantly lower. The lowering of volatilisation by adding Pd is also in agreement with the finding by Carrillo et al. [20] who studied Pt sintering and volatilisation from Pd/Pt Pt deposited on silicon wafer model TEM grids. However, for our supported, washcoated catalysts, at the mol Pd:Pt ratio 0.5:1, there is no effect of the Pd addition on noble metal vaporisation, but a significant effect is seen at higher Pd contents. The presence of alloying in the lowest Pd:Pt ratio is not sufficient to decrease volatilisation. Moreover, it should be noted that of all catalysts examined at T_{vap} = 700 °C, the capturing monolith that possessed the highest ammonia oxidation ability was that downstream of the commercial catalyst.

As discussed in the previous section, it is possible that Pt sintering affects volatilisation and we have therefore studied the particle sizes using XRD and STEM. Moreover, dedicated experiments for the effect of sintering on volatilisation are shown in Section 3.5. Figs. 6b and 7 show that Pd-Pt/Al_2O_3 (Pd:Pt = 0.5:1) also undergoes some sintering. Again, cordierite substrate is the most prominent signal in XRD patterns, and the diamond symbol in Fig. 6 designates peaks characteristic of Pt (111), (220) and (311) [41]. No PdO (34°) peaks are visible in Fig. 6, probably owing to the large cordierite content and possibly due to high dispersion. The diffractograms are replotted in Fig. S7, for easier comparison. This figure shows that there is a small right-shift in Pt(111) in Pd-Pt/Al_2O_3 (Pd:Pt = 0.5:1) compared to Pt/Al_2O_3 at 850 °C, which may be evidence of the presence of Pd (111) [41]. The additional

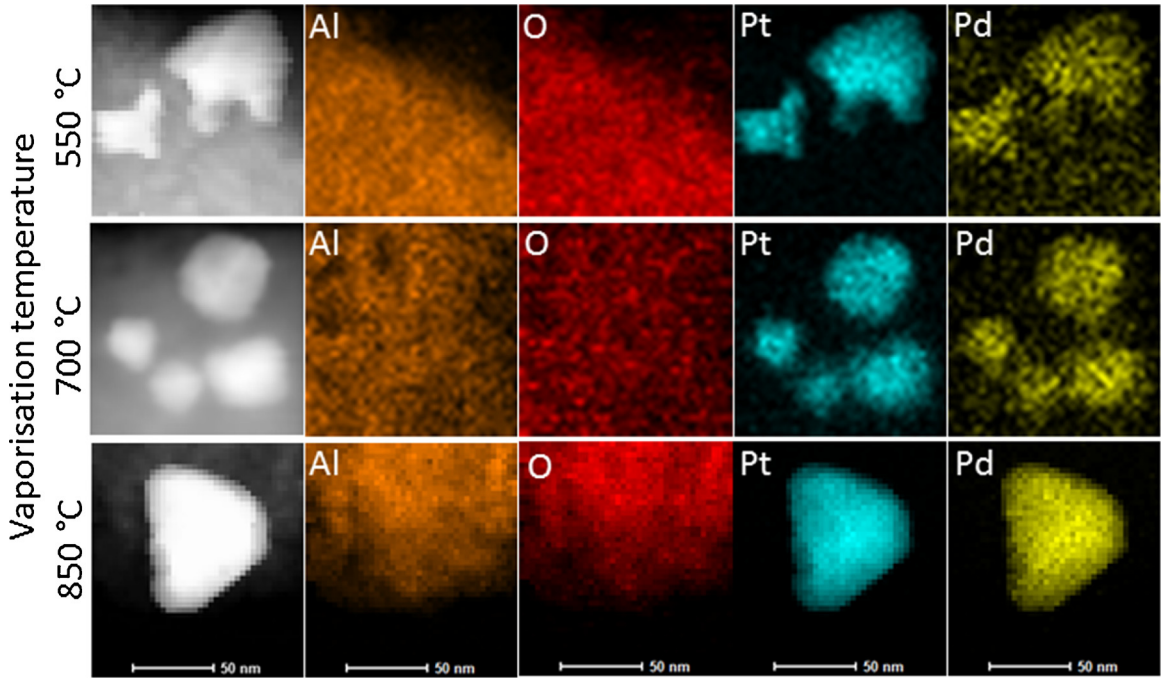

Fig. 8. EDX-TEM mapping of aluminium, oxygen, platinum and palladium compositions for Pd-Pt/Al_2O_3 (Pd:Pt = 0.5:1) subjected to different vaporisation temperatures. Vaporisation with 8% O_2, 5% H_2O, 15 h, 1200 ml/min.

diffractograms in Fig. S8 show that the peak at 40° also increases with Pd content, hence showing that the Pd and Pt are overlapping. As it did for Pt/Al_2O_3, the most prominent noble metal peak increases with vaporisation temperature for Pd-Pt/Al_2O_3 (Pd:Pt = 0.5:1). This indicates that even after addition of Pd, the noble metal crystallite sizes are increasing with temperature. Particle size distributions in Fig. 7 show that for both Pt/Al_2O_3 and Pd-Pt/Al_2O_3 (Pd:Pt = 0.5:1) there is a small increase in the centre of the distribution of particles below 5 nm, from roughly 1.5 to 2.5 nm. However, for particles above 10 nm in size, the centre increases from roughly 12 to roughly 20 nm in the Pt-only catalyst, whereas very few particles > 10 nm are detected in the Pt-Pd (Pd:Pt = 0.5:1) catalyst. The fact that so few particles are over 10 nm in diameter itself suggests that sintering is less severe in presence of Pd, as expected [35].

In summary, the presence of Pd at a mol ratio of Pd:Pt = 0.5:1 reduces mobility of Pt, because less sintering is seen in the bimetallic catalysts. However, the volatilisation remains the same as for Pt only. At higher Pd contents, the volatilisation is significantly decreased.

3.5. Effect of vaporisation duration on noble metal oxide volatilisation

Vaporisation experiments at 700 °C and with 5% H_2O and 8% O_2 were performed for several different lengths of time between 5 h and 40 h for Pt/Al_2O_3 and Pd-Pt/Al_2O_3(Pd:Pt = 0.5:1)-coated cores. Each experiment was performed with a previously un-used parent monolith. Amounts of platinum deposited on the downstream capturing monolith were obtained by analysis of the capturing monoliths through ICP-SFMS, and are plotted in Fig. 9a as a function of the duration of the vaporisation step. Note that Pd was close to or below detection limit for all samples. Overall, Pt volatilisation from Pt/Al_2O_3 and Pd-Pt/Al_2O_3 (Pd:Pt = 0.5:1) increases with time. Correspondingly, ammonia oxidation ability also increases, as show in Fig. 9b. However, the increase is clearly not as fast as that seen with temperature in Fig. 4, and in fact, one should expect a linear relationship to hold if no change in volatilization mechanism (such as decreased volatilization due to decreased dispersion) occurs.

Ammonia oxidation results in Fig. 9b show an overall increasing trend with duration: T_{50} equals 317, 311 and 281 °C for 5, 15 and 40 h over Pd-Pt/Al_2O_3 (Pd:Pt = 0.5:1), so ammonia oxidation ability increases monotonically. For Pt/Al_2O_3, the corresponding numbers are 320, 360 and 273 °C. Note that the oxidation experiment for 15 h corresponds to the upper of the two points in Fig. 10a for Pd-Pt/Al_2O_3 (Pd:Pt = 0.5:1), while the lowest point for Pt/Al_2O_3.This can explain the lower activity for the Pt/Al_2O_3 sample compared to Pd-Pt/Al_2O_3 at this temperature. For the other two samples, the activity is similar for capturing monoliths from evaporation of both Pt/Al_2O_3 and Pd-Pt/Al_2O_3 (Pd:Pt = 0.5:1).

Sintering with vaporisation duration was investigated by XRD and TEM. No effect of longer times on sintering is visible in characteristic Pt/Pd peak sizes in the XRD patterns of Pt/Al_2O_3 and Pd-Pt/Al_2O_3 (Pd:Pt = 0.5:1) (Fig. 10).

The particle size distributions in Fig. 11 however clearly show an increase of particle size, as the centre of the second mode in the bimodal distribution increases from an estimated 12 nm to roughly 20 nm (Pt) or 17 nm (Pd:Pt = 0.5:1). Note that alternative particle size distributions were also obtained for Pt/Al_2O_3 at 40 h, by counting particles in different images for the same sample, and one for a different sample at 40 h, in order to support the results in Fig. 11. These particle size distributions are all shown for comparison in Fig. S10, and support the findings from Fig. 11, as well as the validity of the general procedure of obtaining particle size distributions.

Regarding the different findings from XRD and TEM in terms of particle size, it may be that the effect of sintering at 700 °C for 40 h is such as to cause fewer big particles than sintering at 850 °C for 15 h (results in a previous section), and that this is the reason why no difference is seen with XRD, especially considering the high proportion of cordierite in the sample. Indeed, it is well known that increasing temperature has a much more pronounced effect on sintering than increase of duration [35,49]. It should be noted that Scherrer analysis of XRD data provides a volume-based particle size, while TEM particle sizes are number-based, and that very small particles cannot be “seen” at all with XRD. The lack of difference between XRD patterns at different durations but not at different temperatures is also in line with the fact that all of the 15 h-samples and 40 h-samples analysed had a maximum particle size of 40 nm or lower, while the maximum size went up from 38 nm or lower for T_{vap} = 550 °C to 50 or 74 nm for T_{vap} = 850 °C. Note that the

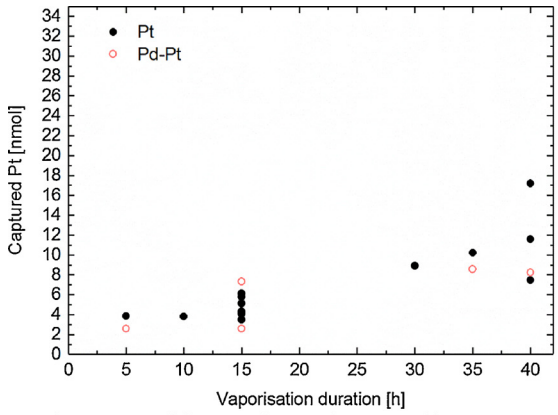

a) Amount of deposited Pt, as determined by ICP-SFMS.

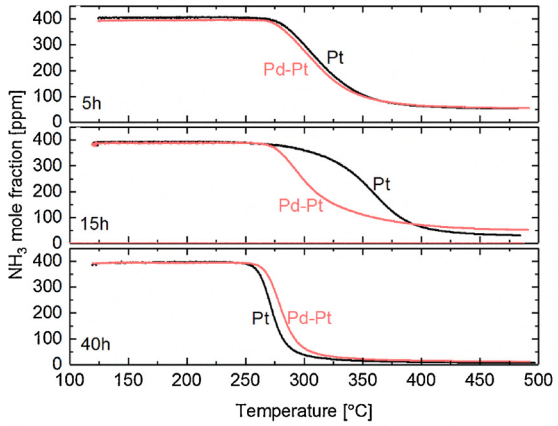

b) NH_3 oxidation ability of deposited noble metal. SV=23390 h^{-1}.

Fig. 9. Effect of vaporisation time on the amount of platinum deposited on a capturing monolith positioned downstream of Pt/Al_2O_3 and $Pd\text{-}Pt/Al_2O_3$ (Pd:Pt = 0.5:1) monoliths, as determined by ICP-SFMS and NH_3 oxidation. Vaporisation with 8% O_2, 5% H_2O, 700 °C, 1200 ml/min, SV = 23,390 h^{-1}. Note that in a) the point for Pd-Pt at 5 h and the lower point at 15 h correspond to ICP-SFMS detection limit.

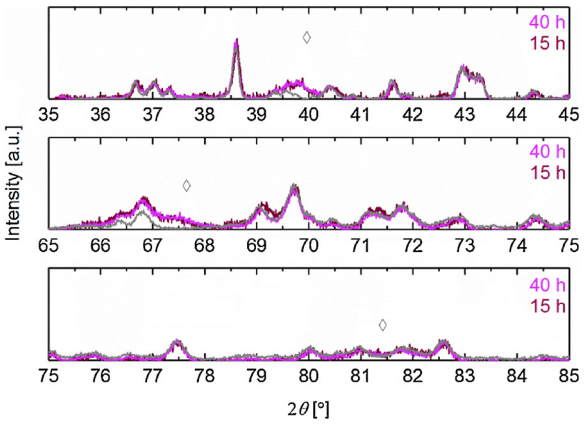

a) Pt/Al_2O_3.

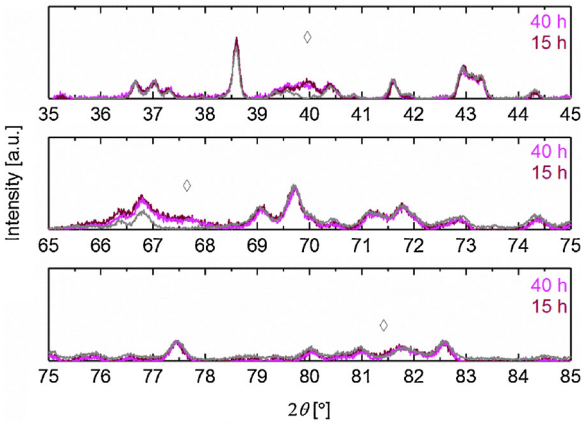

b) $Pd\text{-}Pt/Al_2O_3$ (Pd:Pt=0.5:1).

Fig. 10. X-ray diffractograms of noble metal parent monoliths after vaporisation experiments of different durations. Vaporisation with 8% O_2, 5% H_2O, 700 °C, 1200 ml/min. Grey line – cordierite substrate. ◊ - Pt.

particle size distributions in Figs. 7 and 11 are only shown up to 40 nm for easier visualisation, however, as just mentioned, there are a few particles above this size in the 850 °C-samples, and these few very large particles cause the difference between XRD patterns at different temperatures.

As to the effect of Pd on sintering at different durations, it is expected that the presence of Pd should stabilise against sintering, compared to the Pt-only catalyst, which is consistent with the finding that the second mode of the particle size distribution is centered at roughly 17 nm in the Pd-containing catalysts, as opposed to 20–25 nm when Pt is the only noble metal. In sum, we see evidence of increased particle size for increased durations, and more so for Pt/Al_2O_3 than $Pt\text{-}Pd/Al_2O_3$ (Pd:Pt = 0.5:1).

As mentioned earlier it is possible that lowering of Pt dispersion might lower the amount of volatised platinum, because there is less exposed surface platinum. In order to further study the effect of sintering, a series of consecutive volatilisation experiments at different temperatures was carried out with the same parent monolith. The results are shown in Fig. 12, together with the results obtained for first-time volatilisation from other parent monoliths, where the green markers show the experiments using same parent monolith. It is clear from Fig. 12 that volatilisation from the re-used parent monolith is lessened. This can likely be attributed to increased sintering with each of the repeated vaporisation experiments.

To summarize, our experiments show that increased duration results in increased noble metal vaporisation and thereby an increased ammonia oxidation activity on the capturing monoliths. Moreover, repeated experiments using the same parent monolith show that volatisation is decreased. These results suggests that after use of a DOC for longer times the Pt volatisation may subside due to presence of larger Pt clusters.

4. Conclusions

Noble metal-containing DOCs and DPFs are often placed upstream of an SCR catalyst. Small amounts of noble metals can thus volatilise and deposit on the downstream SCR component, causing noble metal poisoning. In this study, we have reproduced the DOC-upstream-of-SCR configuration in the laboratory, with washcoated model Pt/Al_2O_3, $Pd\text{-}Pt/Al_2O_3$ and Pd/Al_2O_3 catalysts upstream of an alumina-washcoated core and also compared with a commercial DOC. Results confirmed that the poisoning occurs via volatile platinum oxides. Volatilisation from model DOCs increases exponentially with temperature. We observed no difference in volatilisation upon addition of a small amount of Pd (Pd:Pt = 0.5:1), even though Pd stabilised against sintering, likely due to the alloying found by STEM-EDX. For higher Pd:Pt ratios, volatilisation was decreased. To assess the hypothesis that more severe sintering, with a majority of the particles being large, could result in an effect on volatilisation, we performed repeated volatilisation with the same catalyst. The volatilised amounts were smaller than expected, leading us to conclude that sintered particles do indeed volatilise less. The volatilised Pt deposited on alumina-coated “capturing monoliths” in trace amounts (< 35 nmol) and was highly active for NH_3 oxidation,

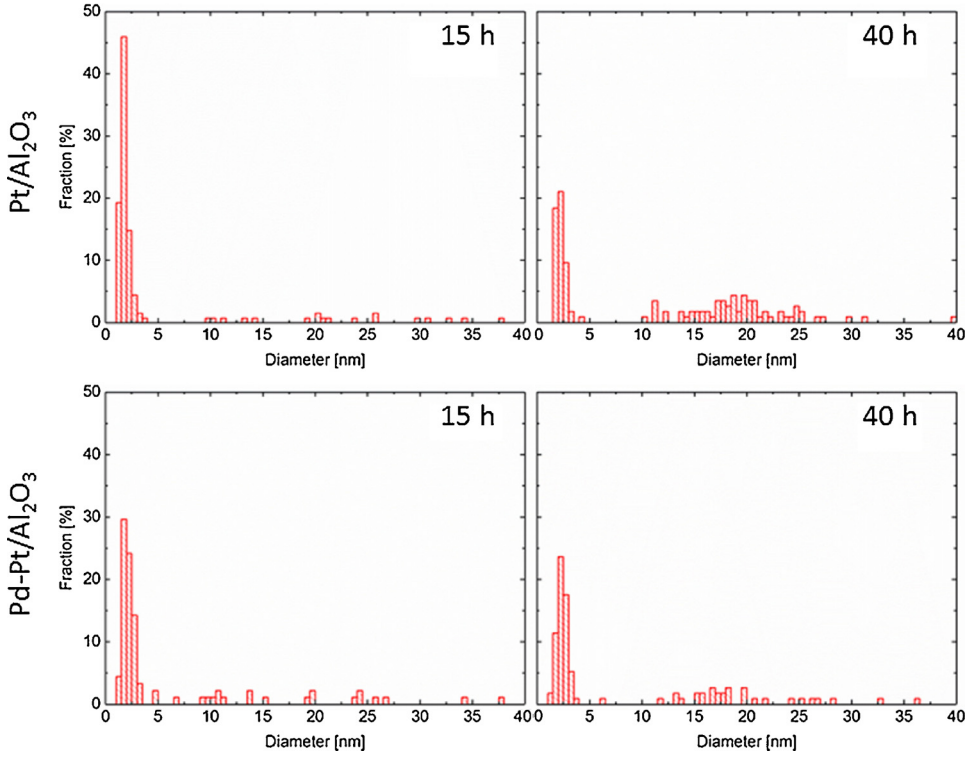

Fig. 11. Particle size distributions for noble metal parent monoliths after vaporisation experiments of different durations. Obtained by counting of particles in micrographs in Figure S9. Vaporisation with 8% O_2, 5% H_2O, 700 °C, 1200 ml/min.

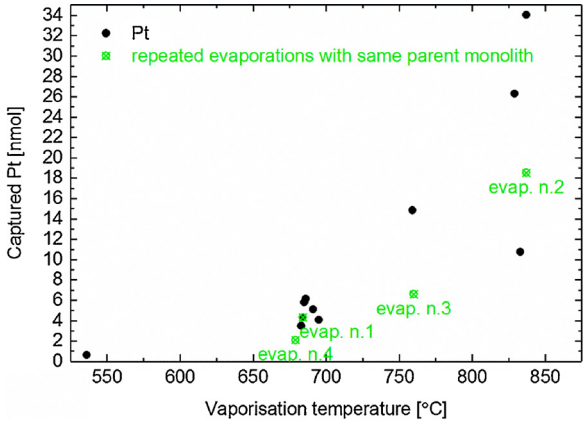

Fig. 12. Effect of repeated vaporisation on the amount of platinum deposited on a capturing monolith positioned downstream of Pt/Al_2O_3 monoliths, as determined by ICP-SFMS. Vaporisation with 8% O_2, 5% H_2O, 15 h, 1200 ml/min. Green markers shows experiments where the same parent monolith is used (For interpretation of the references to colour in this figure legend, the reader is referred to the web version of this article).

but the activity was not stable, with important implications for Pt poisoning in a real aftertreatment system. The deposited Pt is likely finely dispersed, or even in an atomic state, to begin with. During especially the first activity experiment, the NH_3 or CO oxidation increased, which could be caused by agglomeration of platinum atoms.

Acknowledgements

This study was performed at the Division of Chemical Engineering and the Competence Centre for Catalysis, Chalmers University of Technology in collaboration with Cummins Inc. The financial support of Cummins Inc. and the Swedish Research Council (642-2014-5733) are gratefully acknowledged. The Chalmers Materials Analysis Laboratory is acknowledged for instrument access and support and Stefan Gustafsson of the Chalmers Materials Analysis Laboratory is gratefully acknowledged for help with acquisition of STEM-EDX data.

Appendix A. Supplementary data

Supplementary material related to this article can be found, in the online version, at doi:https://doi.org/10.1016/j.apcatb.2018.09.022.

References

[1] F. Alt, A. Bambauer, K. Hoppstock, B. Mergler, G. Tölg, Platinum traces in airborne particulate matter. Determination of whole content, particle size distribution and soluble platinum, Fresenius J. Anal. Chem. 346 (1993) 693–696.
[2] S. Artelt, H. Kock, H. König, K. Levsen, G. Rosner, Engine dynamometer experiments: platinum emissions from differently aged three-way catalytic converters, Atmos. Environ. 33 (1999) 3559–3567.
[3] L. Bencs, K. Ravindra, R. Van Grieken, Methods for the determination of platinum group elements originating from the abrasion of automotive catalytic converters, Spectrochim. Acta Part B At. Spectrosc. 58 (2003) 1723–1755.
[4] P.G. Blakeman, G.M. Brown, S. Chatterjee, A.F. Chiffey, J. Gast, P.R. Phillips, R.R. Rajaram, G. Spreitzer, A.P. Walker, Catalysed substrate monolith, Google Patents (2015).
[5] P.G. Blakeman, G.M. Brown, A.F. Chiffey, J. Gast, P.R. Phillips, R.R. Rajaram, G. Spreitzer, A.P. Walker, Exhaust system for a lean-burn internal combustion engine including SCR catalyst, Google Patents (2016).
[6] S. Rauch, H.F. Hemond, C. Barbante, M. Owari, G.M. Morrison, B. Peucker-Ehrenbrink, U. Wass, Importance of automobile exhaust catalyst emissions for the deposition of platinum, palladium, and rhodium in the northern hemisphere, Environ. Sci. Technol. 39 (2005) 8156–8162.
[7] X. Chen, N. Currier, A. Yezerets, K. Kamasamudram, Mitigation of platinum poisoning of Cu-Zeolite SCR catalysts, SAE Int. J. Engines 6 (2013) 856–861.
[8] G. Cavataio, H.-W. Jen, J.W. Girard, D. Dobson, J.R. Warner, C.K. Lambert, Impact and prevention of ultra-low contamination of platinum group metals on SCR catalysts due to DOC design, SAE Int. J. Fuels Lubr. 2 (2009) 204–216.
[9] H.-W. Jen, J.W. Girard, G. Cavataio, M.J. Jagner, Detection, origin and effect of ultra-low platinum contamination on diesel-SCR catalysts, SAE Int. J. Fuels Lubr. 1 (2008) 1553–1559.
[10] I. Lezcano-Gonzalez, U. Deka, H. van der Bij, P. Paalanen, B. Arstad, B. Weckhuysen, A. Beale, Chemical deactivation of Cu-SSZ-13 ammonia selective catalytic reduction (NH3-SCR) systems, Appl. Catal. B: Environ. 154 (2014) 339–349.

[11] T. Yu, M. Xu, Y. Huang, J. Wang, J. Wang, L. Lv, G. Qi, W. Li, M. Shen, Insight of platinum poisoning Cu/SAPO-34 during NH3-SCR and its promotion on catalysts regeneration after hydrothermal treatment, Appl. Catal. B: Environ. 204 (2017) 525–536.
[12] G.C. Fryburg, H.M. Petrus, Kinetics of the oxidation of platinum, J. Electrochem. Soc. 108 (1961) 496–503.
[13] H. Jehn, High temperature behaviour of platinum group metals in oxidizing atmospheres, J. Less Common Met. 100 (1984) 321–339.
[14] C.B. Alcock, G.W. Hooper, Thermodynamics of the gaseous oxides of the platinum-group metals, Proc. R. Soc. Lond. Ser. A Math. Phys. Sci. 254 (1960) 551–561.
[15] J.A. Moulijn, A. Van Diepen, F. Kapteijn, Catalyst deactivation: is it predictable?: What to do? Appl. Catal. A Gen. 212 (2001) 3–16.
[16] C.B. Alcock, Chapter 1 - Vapour Deposition Processes, Thermochemical Processes, Butterworth-Heinemann, Oxford, 2001, pp. 3–41.
[17] L. Hannevold, O. Nilsen, A. Kjekshus, H. Fjellvåg, Chemical vapor transport of platinum and rhodium with oxygen as transport agent, J. Cryst. Growth 279 (2005) 206–212.
[18] D.M. Mattox, Handbook of Physical Vapor Deposition (PVD) Processing, William Andrew, 2010.
[19] D.M. Mattox, Chapter 10: Atomistic Film Growth and Some Growth-related Film Properties, Handbook of Physical Vapor Deposition (PVD) Processing, William Andrew, 2010, pp. 333–344.
[20] C. Carrillo, A. DeLaRiva, H. Xiong, E.J. Peterson, M.N. Spilde, D. Kunwar, R.S. Goeke, M. Wiebenga, S.H. Oh, G. Qi, Regenerative trapping: how Pd improves the durability of Pt diesel oxidation catalysts, Appl. Catal. B: Environ. 218 (2017) 581–590.
[21] D. Sobczyk, E. Hensen, A. De Jong, R. Van Santen, Low-temperature ammonia oxidation over Pt/γ-alumina: the influence of the alumina support, Top. Catal. 23 (2003) 109–117.
[22] R. Kraehnert, M. Baerns, Morphology changes of Pt-foil catalyst induced by temperature-controlled ammonia oxidation near atmospheric pressure, Appl. Catal. A Gen. 327 (2007) 73–81.
[23] L. Gang, B.G. Anderson, J. van Grondelle, R.A. van Santen, NH3 oxidation to nitrogen and water at low temperatures using supported transition metal catalysts, Catal. Today 61 (2000) 179–185.
[24] J.J. Ostermaier, J.R. Katzer, W.H. Manogue, Platinum catalyst deactivation in low-temperature ammonia oxidation reactions: I. Oxidation of ammonia by molecular oxygen, J. Catal. 41 (1976) 277–292.
[25] J. Ostermaier, J. Katzer, W. Manogue, Crystallite size effects in the low-temperature oxidation of ammonia over supported platinum, J. Catal. 33 (1974) 457–473.
[26] T.K. Hansen, Development of New Diesel Oxidation and NH_3 Slip Catalysts, Technical University of Denmark, 2017 PhD thesis.
[27] R. Krähnert, Ammonia Oxidation Over Polycrystalline Platinum: Surface Morphology and Kinetics at Atmospheric Pressure, Technische Universität Berlin, 2005 PhD thesis.
[28] T.K. Hansen, M. Høj, B.B. Hansen, T.V. Janssens, A.D. Jensen, The effect of Pt particle size on the oxidation of CO, C3H6, and NO over Pt/Al2O3 for diesel exhaust aftertreatment, Top. Catal. 60 (2017) 1333–1344.
[29] A.C.M. van den Broek, Low Temperature Oxidation of Ammonia Over Platinum and Iridium Catalysts, Technische Universiteit Eindhoven, 1998.
[30] H. Schäfer, A. Tebben, Gleichgewichtsmessungen im system platin—sauerstoff gasförmiges platindioxyd, Zeitschrift für anorganische und allgemeine Chemie 304 (1960) 317–321.
[31] H. Jehn, Platinum losses during high temperature oxidation, J. Less Common Met. 78 (1981) 33–41.
[32] C.J. Adkins, Equilibrium Thermodynamics, Cambridge University Press, 1983.
[33] J. Chaston, The oxidation of the platinum metals, Platin. Met. Rev. 19 (1975) 135–140.
[34] P.S. Dhillon, M.P. Harold, D. Wang, A. Kumar, S. Joshi, Hydrothermal aging of Pt/Al_2O_3 monolith: washcoat morphology degradation effects studied using Ammonia and propylene oxidation, Catal. Today (2017), https://doi.org/10.1016/j.cattod.2017.12.023 In press.
[35] A. Russell, W.S. Epling, Diesel oxidation catalysts, Catal. Rev. 53 (2011) 337–423.
[36] P.N. Plessow, F. Abild-Pedersen, Sintering of Pt nanoparticles via volatile PtO2: simulation and comparison with experiments, ACS Catal. 6 (2016) 7098–7108.
[37] A.D. Benavidez, L. Kovarik, A. Genc, N. Agrawal, E.M. Larsson, T.W. Hansen, A.M. Karim, A.K. Datye, Environmental transmission electron microscopy study of the origins of anomalous particle size distributions in supported metal catalysts, ACS Catal. 2 (2012) 2349–2356.
[38] A.K. Datye, Q. Xu, K.C. Kharas, J.M. McCarty, Particle size distributions in heterogeneous catalysts: What do they tell us about the sintering mechanism? Catal. Today 111 (2006) 59–67.
[39] E.D. Goodman, J.A. Schwalbe, M. Cargnello, Mechanistic understanding and the rational design of sinter-resistant heterogeneous catalysts, ACS Catal. 7 (2017) 7156–7173.
[40] F. Grillo, H. Van Bui, J.A. Moulijn, M.T. Kreutzer, J.R. van Ommen, Understanding and controlling the aggregative growth of platinum nanoparticles in atomic layer deposition: an avenue to size selection, J. Phys. Chem. Lett. 8 (2017) 975–983.
[41] T.R. Johns, J.R. Gaudet, E.J. Peterson, J.T. Miller, E.A. Stach, C.H. Kim, M.P. Balogh, A.K. Datye, Microstructure of bimetallic Pt–Pd catalysts under oxidizing conditions, ChemCatChem 5 (2013) 2636–2645.
[42] C. Lentz, S.P. Jand, J. Melke, C. Roth, P. Kaghazchi, DRIFTS study of CO adsorption on Pt nanoparticles supported by DFT calculations, J. Mol. Catal. A Chem. 426 (2017) 1–9.
[43] N. Sheppard, C. De La Cruz, The reliability of vibrational spectroscopy as a means of identification of the structures of chemisorbed species on metal surfaces: the cases of CO, NO and C2 hydrocarbon surface species, Catal. Today 70 (2001) 3–13.
[44] A.I. Serykh, O.P. Tkachenko, V.Y. Borovkov, V.B. Kazansky, K.M. Minachev, C. Hippe, N.I. Jaeger, G. Schulz-Ekloff, Characterization of silica-gel supported Pt-Cu alloy particles prepared [italic v (to differentiate from Times ital nu)]ia the sol-gel technique, Phys. Chem. Chem. Phys. 2 (2000) 2667–2672.
[45] A. Boubnov, A. Gänzler, S. Conrad, M. Casapu, J.-D. Grunwaldt, Oscillatory CO oxidation over Pt/Al 2 O 3 catalysts studied by in situ XAS and DRIFTS, Top. Catal. 56 (2013) 333–338.
[46] R.K. Brandt, M. Hughes, L. Bourget, K. Truszkowska, R.G. Greenler, The interpretation of CO adsorbed on Pt/SiO2 of two different particle-size distributions, Surf. Sci. 286 (1993) 15–25.
[47] H. Shinjoh, H. Muraki, Y. Fujitani, Effect of Severe Thermal Aging on Noble Metal Catalysts, Studies in Surface Science and Catalysis, Elsevier, 1991, pp. 617–628.
[48] J. Arblaster, Vapour pressure equations for the platinum group elements, Platin. Met. Rev. 51 (2007) 130–135.
[49] D. Chan, S. Tischer, J. Heck, C. Diehm, O. Deutschmann, Correlation between catalytic activity and catalytic surface area of a Pt/Al2O3 DOC: an experimental and microkinetic modeling study, Appl. Catal. B: Environ. 156 (2014) 153–165.